Chemical Engineering Science 248 (2022) 117152

Contents lists available at ScienceDirect

Chemical Engineering Science

journal homepage: www.elsevier.com/locate/ces

# Studying droplet retention in porous media by novel microfluidic methods

Ilgar Azizov, Marcin Dudek, Gisle Øye *

*Ugelstad Laboratory, Department of Chemical Engineering, Norwegian University of Science and Technology (NTNU), 7491 Trondheim, Norway*

## HIGHLIGHTS

- Microfluidic methodology for retention studies was demonstrated.
- Droplet retention in porous media was examined at the capillary level.
- Monodisperse and tailored polydisperse emulsions were tested.
- Droplet size played the major role in the droplet retention.
- The demonstrated method provides flexibility for testing various emulsion systems.

## GRAPHICAL ABSTRACT

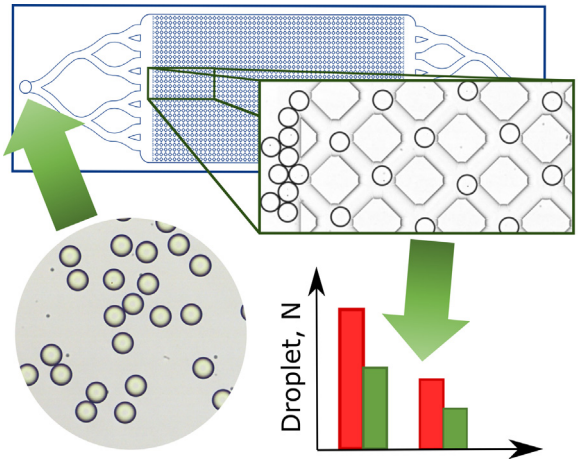


## ARTICLE INFO

*Article history:*
Received 12 July 2021
Received in revised form 13 September 2021
Accepted 25 September 2021
Available online 28 September 2021

*Keywords:*
Microfluidics
Droplet retention
Produced water re-injection
Emulsions
Porous media
Pore clogging

## ABSTRACT

Transport of oil droplets through porous media is an important topic in the oil and gas industry. Oil droplets that are present in produced water contribute to injectivity decline during re-injection due to retention in pores. In the literature, the retention phenomenon is typically studied by means of core/packed bed flooding, which struggles to provide a simple and inexpensive way to visualize retention events at the pore scale. This paper demonstrates a microfluidic method for studying the transport of dilute oil-in-water emulsions through porous media. The method allows identification of every single retention event at the capillary level and quantitative analysis of the spatial distribution of the retained droplets over pore volumes injected. Experiments were carried out for monodisperse and tailored polydisperse emulsions. Moreover, several droplet sizes, flow rates and dispersed phase concentrations were tested. The results showed that the droplet size has a dramatic effect on the pore clogging. Droplets that are larger than pore throats underwent complete retention, while droplets that are smaller than pore throats showed little to no retention in the monodisperse emulsion experiments. Additionally, the experiments with polydisperse emulsions showed that the larger droplets are facilitators for the retention of the smaller droplets, and the latter are unlikely to experience significant retention independently of the former. The flow rates affected flow re-entry mechanisms of the larger droplets, while for the smaller droplets it influenced only the number of retention events. It was identified that dispersed phase concentration has a significant effect in experiments with limited pore volumes injected. At low concentration, the obtained statistical sample was not sufficiently large to unravel the trends. The developed method

* Corresponding author.
*E-mail addresses:* ilgar.azizov@ntnu.no (I. Azizov), marcin.dudek@ntnu.no (M. Dudek), gisle.oye@ntnu.no (G. Øye).

https://doi.org/10.1016/j.ces.2021.117152

presents a solid foundation for further experiments and developments in microfluidic studies of the emulsion transport.



## 1. Introduction

There are large amounts of water co-produced with oil and gas during the recovery of hydrocarbons. The amount of produced water (PW) depends on the stage of recovery and typically increases with the lifetime of the field. Worldwide, on average, there are 4 barrels of water produced per 1 barrel of oil (Dudek et al., 2020b). Produced water comprises a variety of dispersed and dissolved components, originating both from reservoir and processing operations, which can be environmentally harmful (Fakhru'l-Razi et al., 2009). Typically, on the offshore installations PW is either discharged into the sea or re-injected back into the reservoir. The discharge of water is a prevailing approach of produced water management. According to the current legislation for the Norwegian Continental Shelf, the concentration of dispersed oil in PW must not exceed 30 mg/l when the water is discharged. However, regulatory authorities in Europe urge oil companies to decrease the discharge limit to 15 mg/l (European Commission, 2019). This would increase the cost of treatment and make the discharge more expensive, which shifts the attention to produced water re-injection (PWRI) as a more environmentally friendly and potentially economic option.

Although PW undergoes treatment before re-injection, there are still dispersed particles and droplets present in the water as complete purification is impractical from the cost point of view (Palsson et al., 2003). These dispersed components clog the pores of a formation when PW is re-injected, which causes an injectivity decline of wells over time (Tipura et al., 2013). Thus, a compromise must be made between the cost of the treatment and the expenses associated with the potential damage and remediation (Palsson et al., 2003). Field reports of produced water re-injection indicate that the current practice of water quality specification is variable and often deficient in limiting the injectivity decline. In some cases, on site coreflooding tests are deployed to obtain representative data for the flooded reservoir (Costier et al., 2009; Souza et al., 2005) , while in other cases a rule of thumb is utilized – up to 10 ppm and up to 40 ppm for total suspended solids and oil concentration respectively (Rossini et al., 2020). On the other hand, some reports suggest that the properties of reservoirs and suspended components must be considered when setting specifications of injection water (Evans, 1994; Rossini et al., 2020).

The process of injectivity impairment by suspended particles or droplets is characterized by the formation of an external filter cake at the face of the well and an internal filter cake in the near wellbore region (Ochi and Oughanem, 2018; Pang and Sharma, 1997). The transport and retention of solids and droplets in porous media is often described by the deep bed filtration theory (Civan, 2007; Soo and Radke, 1986). According to this theory, the retention of particles occurs by two mechanisms: straining capture and interception capture. Straining happens when a particle is of comparable size to a pore throat, so the particle can lodge in the constriction and clog it. Interception capture happens when particles are captured on the surface of a pore wall due to surface forces (Herzig et al., 1970). The two mechanisms can complement each other. For example, a particle that is smaller than a constriction can be captured by surface forces, reducing the effective pore area. Then, another particle that is larger than the remaining effective area would clog the pore completely by the straining mechanism. The literature suggests that solid particles larger than 1/3 of pore size build an external filter cake, while particles in the range between 1/3 and 1/14 of pore size form an internal filter cake (Abrams, 1977; van Oort et al., 1993). The retention of droplets is similar to the one of particles; however, unlike particles, droplets are deformable and can be squeezed through a constriction if the pressure across the pore throat is large enough to overcome the capillary forces retaining the droplet.

In the literature, experimental studies of the retention phenomenon are typically done by core plug or packed bed flooding (Ali et al., 2011; Błaszczyk et al., 2016; Ding et al., 2020; Guillen et al., 2012b; Yu et al., 2017). Due to the limitation of flooding techniques when it comes to the visualization of pore scale events, most of the conclusions regarding the damage of the porous media are based on pressure data (Vaz et al., 2017) and dispersed phase concentrations at the inlet and the outlet of a sample (Rousseau et al., 2007). The lack of visualization limits advances in the field as it could give a better understanding of the plugging phenomenon. Micro-computed tomography could be applied to see inside the samples (Mikolajczyk et al., 2018); however, this technique is expensive and complex to implement. A more convenient technique that could provide insight into the pore scale phenomena and give good reproducibility of results is microfluidics (Jahanbakhsh et al., 2020). Microfluidic studies of flow in porous media give an advantage over packed bed/core flooding when it comes to visualization and flexibility for testing various conditions, e.g. flow conditions (Liu et al., 2019a), wettability (Saadat et al., 2021; Sandengen et al., 2016; Schneider and Tabeling, 2011), pore size and geometry (Saadat et al., 2020; Xu et al., 2014). Retention of solid particles has also been successfully investigated using microfluidics in several studies (Auset and Keller, 2006; (van de Laar et al., 2016; Liu et al., 2019a; Wyss et al., 2006).

In this work, we explored and utilized microfluidics as a technique to investigate clogging of pores by droplets, by studying the transport of monodisperse and polydisperse model oil emulsions through a uniform network of channels. We systematically varied droplet sizes, injection rates, and dispersed phase concentration. Image-based quantitative and qualitative analyses were performed to follow the progress of droplet retention over pore volumes injected and the distance from the injection point. Firstly, the effect of droplet size and injection rate on pore clogging is discussed in the context of monodispersed emulsions. Afterwards, the influence of the dispersed phase concentration on the interpretation of the observations is analyzed. Then, the results of experiments with tailored polydisperse emulsions are presented. Lastly, the proposed method is compared to other techniques, and advantages and disadvantages of the method are examined. To the best of our knowledge, this is the first time a study of droplet retention in porous media is carried out for dilute oil-in-water emulsions using a microfluidic approach.

## 2. Experimental Section

### 2.1. Fluids and chemical additives

#### 2.1.1. Fluid properties

A surfactant solution was used as a continuous phase during the experiments to limit coalescence between droplets. The solution was prepared by dissolving 0.4 mM of the non-ionic surfactant Tween 20 (CMC = 0.06 mM at 20-25℃) (Sigma Aldrich, Germany)

and 17 mM of laboratory grade NaCl (VWR, USA) in deionized water (Millipore Simplicity Systems, Germany).

A mixture of two model oils, namely dodecane and 1-bromododecane, was used as a dispersed phase. The model oils were mixed to mitigate the gravity separation of the emulsion during the flooding experiments. It was experimentally found that the mixture with the density of 1002.00 kg/m$^3$ is optimal (Fig, S1 and Fig S2 in Supplementary Information). The density of the continuous phase was measured to be 999.11 kg/m$^3$, while dodecane and 1-bromododecane were measured to be 748.96 kg/m$^3$ and 1040.24 kg/m$^3$ respectively. A mixture composed of 13.13 v% of dodecane and 86.87 v% of 1-bromododecane resulted in the density of 1002.00 kg/m$^3$. The mixture was prepared by weighing, and the actual density of the obtained sample was measured to be 1001.87 kg/m$^3$, which was considered sufficiently accurate. All the densities were measured using a density meter at 20℃ (DMA 5000 M, Anton Paar, Austria).

Interfacial tension (IFT) between two phases was measured using a spinning drop tensiometer (SVT20, dataphysics, Germany) at 20 °C. Since the continuous and dispersed phase had almost the same density it was not possible to measure the IFT using the prepared mixture of model oils. Instead, a 50.50 v% mixture of dodecane and 1-bromododecane with the density of 894.87 kg/m$^3$ was used, which allowed to perform an accurate measurement. It is believed that the measured value is representative of the system used for experiments as the surfactant molecules would saturate the interface at the used concentration. The IFT was measured to be 4.6 mN/m.

#### 2.1.2. Emulsions

Two types of emulsions were utilized in the experiments: monodisperse emulsions and a polydisperse emulsion comprising droplets of three sizes. The oil-in-water emulsions were generated using a microfluidic droplet generator (Section 2.2.1). In total, six monodisperse emulsions were prepared with the following variables: droplet sizes of 15 μm, 30 μm and 42 μm; and two dispersed phase concentrations of 500 ppm and 1500 ppm. The polydisperse emulsion contained droplets of 15 μm, 30 μm, and 42 μm with the total dispersed phase concentrations of 1500 ppm. The polydisperse emulsion contained approximately equal numbers of droplets of each size. All the emulsions were produced in 750 μl batches.

### 2.2. Microfluidic chips and setup

#### 2.2.1. Droplet generators

Cross-flow and flow-focusing microfluidic droplet generators were utilized for emulsification. The microfluidic chips were made of glass and are hydrophilic. The chips were manufactured by Micronit Microtechnologies B.V. (The Netherlands). The flow-focusing chip was designed by the manufacturer (DGFF.10), while the cross-flow chip was designed inhouse (Dudek et al., 2020a). The cross-flow geometry (T-junction) was used for generation of 30 μm and 42 μm size droplets. The T-junction was formed by two 100 μm wide and 45 μm deep inlet channels, which was followed by 500 μm wide and 45 μm deep channel. The flow-focusing geometry was used for the droplets of 15 μm size. The nozzle size of the flow focusing device was 10 μm, while the height of the channels was 17 μm.

#### 2.2.2. Micromodel (Porous medium)

Microfluidic chips representing a porous medium by a uniform network of channels were used in this work. The chips were designed and manufactured by Micronit Microtechnologies B.V. The micromodels were made of glass and are hydrophilic. A detailed description of the micromodel can be found elsewhere (Pradhan et al., 2019), while a brief description is provided here for practical reasons. The schematic of the micromodel can be found in Supplementary Information (Fig. S3). The network of channels is 10 mm × 20 mm and contains 10,050 pores (coordination number = 4). The network is preceded and followed by a lateral channel of 10 mm × 0.5 mm. The depth of all channels and the network is 20 μm. The width of the pore bodies is 90 μm, while the width of pore throats is 50 μm (Fig. S4). Fluids enter the chip through a conical inlet followed by an inlet channel that is successively bifurcated three times. The last bifurcation step results in 8 channels. These channels are evenly connected to the lateral channel allowing uniform transport of fluids to the network. The outlet part of the chip is symmetrical to the inlet part.

#### 2.2.3. Setup

During the droplet generation and emulsion flooding, the chips were placed into a chip holder (Fluidic Connect Pro, Micronit Microtechnologies B.V., The Netherlands) and connected to the flow device through FFKM ferrules and an FEP tubing (ID 250 μm, IDEX Health & Science). Syringe pumps (neMESYS mid-pressure module 1000 N and low-pressure module 290 N, Cetoni GmbH, Germany) were used to move the liquids.

The micromodel was imaged using a 4MP color high-speed camera (FASTCAM Mini WX100, Photron, Japan) connected to an inverted microscope (Eclipse Ti2-U, Nikon, Japan). The microscope is equipped with a motorized stage and a focus drive (OptiScan III, Prior Scientific, UK). The camera and the motorized components of the microscope were coupled through a LabVIEW code, which allowed to fully automate imaging of the micromodel during the experiments.

### 2.3. Experimental procedure

The experiments consisted of two interconnected parts: droplet generation and emulsion flooding. All the experiments were performed at room temperature (approx. 20 °C).

#### 2.3.1. Droplet generation

Since the droplet generators have large throughputs, the generated emulsions had dispersed phase concentrations significantly higher than required and were diluted with the continuous phase. The emulsion volumes generated on the chip and the volumes of the continuous phase added to obtain the required concentrations (Section 2.1.2.) can be found in Supplementary Information (Table S1). Table 1 summarizes the flow rates used for droplet generation and the corresponding droplet sizes. The emulsions were collected outside the chip through an FEP tubing (ID 250 μm, length = 10 cm) and afterwards diluted by the pre-calculated volumes of the dispersed phase to reach desired concentrations.

#### 2.3.2. Emulsion flooding

The flooding was performed by withdrawal of the emulsion rather than injection. The setup is illustrated in Fig. 1. A glass funnel connected to the inlet of the microfluidic chip was used to store and dispense the emulsion, while the outlet of the microfluidic chip was connected to the syringe pump. This approach allowed

**Table 1**
Flow rates and chip designs used to generate droplets.

| Chip design | Continuous phase flow rate [μl/min] | Dispersed phase flow rate [μl/min] | Droplet diameter [μm] |
|---|---|---|---|
| Flow-focusing | 15 | 0.3 | 15 |
| Cross-flow | 275 | 3 | 30 |
| Cross-flow | 450 | 3 | 42 |

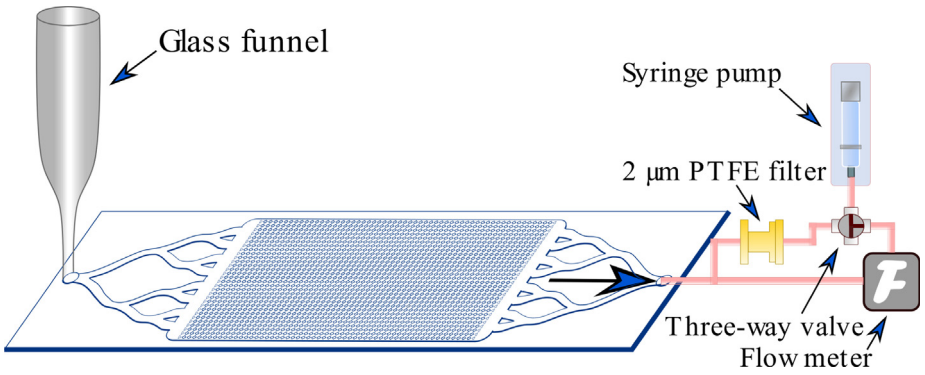


**Fig. 1.** Diagram of the flooding setup. Objects are not drawn to scale. Chip holder is not illustrated.

the storage of an emulsion closer to the chip and eliminated any undesired phenomena associated with the transport of the emulsion through long tubing. The funnel was made by shortening the tip and the body of a Pasteur glass pipette and connected to the chip through an FFKM ferrule. The volume of the funnel was approximately 1 ml. An analog flow meter (MFS2, ElveFlow, France) was connected to the setup during flooding to verify constant flow rates.

All the tubes were flushed with the continuous phase before connecting to the micromodel to avoid air bubbles in the system. The micromodel was saturated with the continuous phase through a 2 μm PTFE filter at 250 μl/min. Afterwards, the funnel was filled with 250 μl of continuous phase using a micropipette. The emulsion from the droplet generator was collected directly into the funnel and diluted as described in Section 2.3.1. The emulsion was gently stirred using a syringe needle to achieve homogeneity. Lastly, the needle was lowered down to the bottom of the funnel tip, and 200–250 μl of emulsion was withdrawn with a syringe to ensure homogeneity in the funnel tip as well. Table 2 provides the summary of all experimental conditions. All the experiments were performed twice to ensure repeatability. The droplet generation chips were cleaned after each experiment by sonication successively in four liquids for 15 min each: toluene/acetone mixture (2:1 v/v), 2% aqueous solution of Decon 90™, isopropanol and de-ionized water. The micromodels were backflushed at 150 μl/min after each experiment with pure continuous phase to remove the dispersed phase from the network. Afterwards, the micromodel was cleaned by successively injecting de-ionized water, isopropanol, and again de-ionized water for at least 20 PV each. In the end, both micromodels and droplet generators were baked in an ashing furnace for 6 h at 450 °C. The glass funnel was cleaned manually by de-ionized water, isopropanol, and again de-ionized water, and afterwards dried in a heating cabinet at 60 °C overnight.

### 2.3.3. Data acquisition

The micromodel was imaged by obtaining a sequential continuous grid of images using the motorized microscope stage. This approach was opted to address the spatial scale mismatch between the field of view of the microscope and the network. The motivation to cover a large area of the network comes from the need to obtain good statistical sampling and to capture rare droplet retention events. The complete imaging was performed on per 2 PV basis for monodisperse emulsions and 4 PV basis for polydisperse emulsion experiments, which was empirically found as an optimal resolution for the data collection. The area of the network that can be covered per defined amount of time is limited by the movement speed of the motorized stage. Therefore, the covered area varied between experiments depending on the injection rate and magnification Table 2. For the purpose of image analysis, a pair of images were taken at each grid position within the same sequence. The time interval between the images in a pair varied depending on the flow rate to allow image analysis. Table S2 summarizes the information about the grid sizes and motorized stage movements.

## 2.4. Image processing and analysis

The image processing and analysis process was built on analyzing image pairs as all the objects on single images appear static precluding identification of the retained droplets. Image pairs enabled distinguishing captured and moving droplets.

**Step 1: Removal of moving droplets.** First, the acquired images were converted from 24-bit RGB to 8-bit grey scale, where the structure of the chip had intensities around 255 (white pixels), while the water–oil interfaces and channel edges below 220 (darker pixels). Afterwards, the temporal differencing technique was applied to the image pairs to extract moving droplets from the images. Fig. 2a and Fig. 2b show an image pair taken at the same grid position with 1320 ms interval, image *i* and image *i + t* respectively. It can be seen from the image pair that some droplets on the image *i + t* changed their position with respect to image *i*. This creates a difference in the intensity of foreground pixels ($I_f$) representing moving objects and the intensity of background pixels ($I_b$) representing static objects (the chip structure and the retained droplets). When image *i + t* is subtracted from image *i*, all the background pixels of image *i + t* obtain a value around 0 due to a matching $I_b$, while the foreground pixels obtain new values of $I_b$ - $I_f$. The result of this operation is a new image revealing foreground pixels

**Table 2**
Conditions and emulsions tested in the experiments.

| Type | Droplet size [μm] | Flow rate [μl/min] | Concentration [ppm] | Capillary number | Zones imaged | PVs |
|---|---|---|---|---|---|---|
| Monodisperse | 15 | 0.125 | 500/1500 | $4.30*10^{-6}$ | 1 + 2 + 3 + 4 | 10 |
| | 15 | 0.25 | 500/1500 | $8.62*10^{-6}$ | 1 + 2 + 3 + 4 | 10 |
| | 30/ (15) | 1 | 500/1500 | $3.44*10^{-5}$ | 1 + 2 + 3 + 4/ (1 + 2) | 40/ (10) |
| | 30/42 | 2 | 500/1500 | $6.89*10^{-5}$ | 1 + 2 | 40 |
| | 30/42 | 4 | 500/1500 | $1.37*10^{-4}$ | 1 + 2 | 40 |
| Polydisperse | 15 + 30 + 42 | 2 | 1500 | $6.89*10^{-5}$ | 1 + 2 | 40 |
| | 15 + 30 + 42 | 4 | 1500 | $1.37*10^{-4}$ | 1 + 2 | 40 |

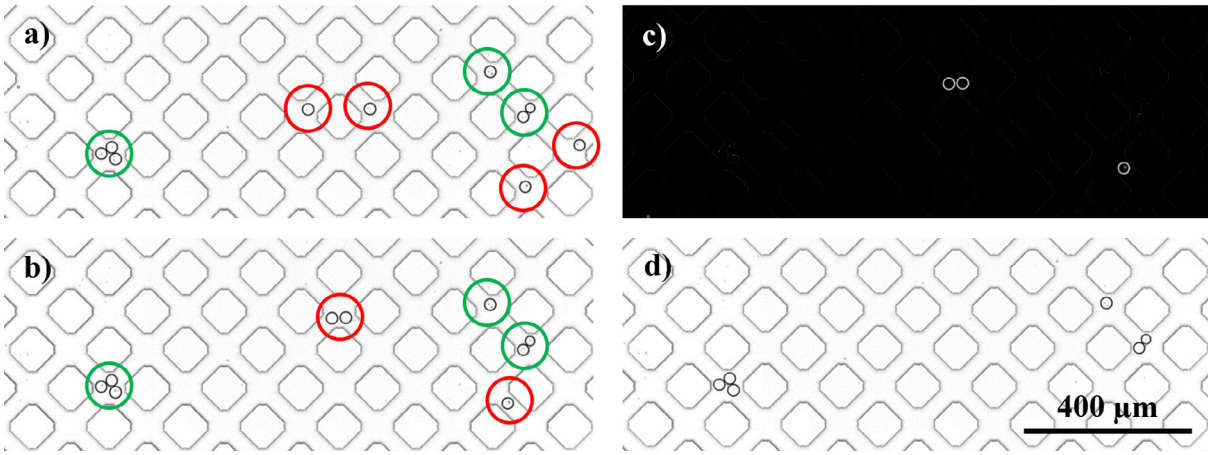


**Fig. 2.** Image analysis process: (a) image «i» in the pair of images; (b) image «i + t» in the pair of images, taken 1320 ms after image "i"; (c) the result of the subtraction of image «i + t» from image «i» displaying moving droplets of image «i + t»; and d) the final image containing only captured droplets.

of image i + t (Fig. 2c). As the next step, the new image is summed with image *i + t*. In this case the pixels which had a value of 0 obtain intensity values of 0 + $I_b$, while the foreground pixels obtain intensities of $I_b$ - $I_f$ + $I_f$ (around 255), which causes moving droplets to disappear from the image (Fig. 2d).

**Step 2: Droplet detection.** Circular Hough transform (Atherton and Kerbyson, 1999) was applied to the images using a built-in Matlab function to automatically detect droplets on per image basis. The Matlab function returned radii of detected circles, pixel-wise positions of circles centers, and the number of detected circles per image. The obtained data was linked to the grid position of an analyzed image for the purpose of further processing. Occasionally, the function identified parts of the chip structure as circles. In order to avoid inclusion of such instances into the results, the data was filtered based on the expected droplet radius.

**Step 3: Network zonation.** In conventional flooding experiments, there are typically discrete measurements of a pressure drop over the length of long cores or packed beds (Fig. 3). This breaks down a sample into sections which enables estimation of permeability in every section independently. The obtained series of permeabilities allows to follow the development of the damage caused by the dispersed components across a sample over time. In this paper, a similar zone-based approach was utilized to allow comparison of results with the data in the literature and enable validation of the method. The micromodel was organized into four area-wise equal zones as illustrated in Fig. 3. Zone 1 included the frontal part of the network and its surface, where the external filter cake normally forms, while zone 2, 3, and 4 included subsequent parts of the network. The number of zones and images comprising a zone varied between experiments, while the area covered per zone was kept comparable. Table 2 presents the number of zones with respect to experimental condition. Table S2 in Supplementary Information shows the details of zonation (area covered, etc.). The grid position of the image pairs was utilized to assign the data obtained in Step 2 to a corresponding zone. The data was reported on per zone basis.

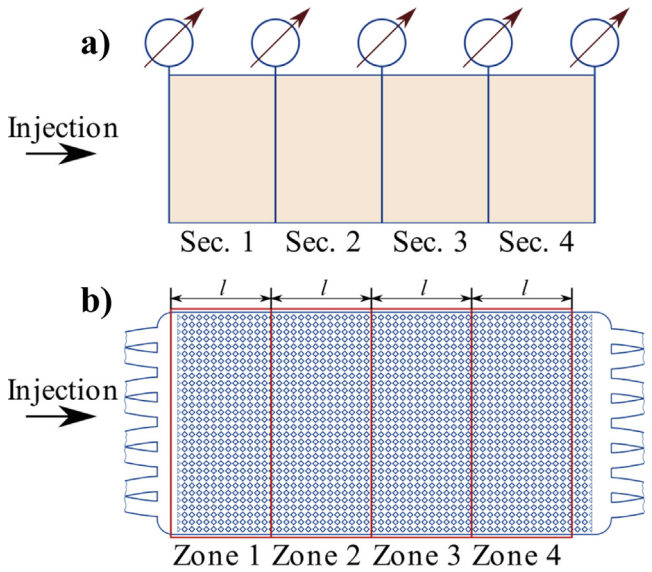


**Fig. 3.** (a) Schematic of a core plug sectioninig for pressure drop measurments; (b) illustration of micromodel zonation for reporting the droplet capture data.

## 3. Results and discussion

In a typical injection scenario in sandstone reservoirs, the capillary number in a limited region around a wellbore is in the order of $10^{-4}$-$10^{-5}$ (Jin and Wojtanowicz, 2014), while deeper in the reservoir, outside that region, the capillary number is about $10^{-7}$ (Mendez, 1999). In this paper, the used flow rates correspond to the capillary numbers representing the near wellbore region (Table 2).

Droplets that have a larger diameter than the channel depth are squeezed during the transport through the micromodel, namely 30 µm and 42 µm. Thus, there is a friction force acting on the droplets that slows them down with the most noticeable effect being in the inlet channel due to its width. An estimation of the velocity loss in the inlet channel can be found in Supplementary Information (Fig. S5). It was observed that the velocity loss increased as the flow rate decreased. Moreover, the loss was slightly greater for 42 µm droplets than 30 µm droplets at 2 µl/min rate, while at 4 µl/min the loss was similar for both droplet sizes. At 1 µl/min flow rate, 42 µm droplets were experiencing high drag in the inlet channel; therefore, this combination of conditions was excluded from the experimental matrix. Droplet sizes larger than 42 µm were not considered for the same reason. The squeezed droplets obtained ellipsoid-like cross-sections. The maximum diameter of the cross-section for a squeezed 42 µm droplet was estimated to be 52 µm which is slightly larger than the width of a pore throat, while for a 30 µm droplet the maximum diameter was 40 µm. However, it is important to mention that although the surface of the channels is relatively smooth there are protrusions at the

throat to pore body connection causing surface irregularity. This irregularity constricts a pore throat at the entrance point by approximately 8 μm. Further in the text the original (non-squeezed) droplet sizes are used for consistency with Section 2. All in all, the transport of droplets that are comparable to the size of pore throats and smaller were studied at the flow rates representative of near wellbore conditions.

### 3.1. The effect of drop-to-pore size ratio

The experimental results showed a significant effect of drop-to-pore size ratio on the droplet capture rate. Fig. 4 presents the total number of retained droplets after 40 PV of flooding as a function of droplet size at the flow rate of 4 μl/min and 1500 ppm dispersed phase concentration. It is important to note that the external filter cake is included into the data; however, the number of droplets captured at the entrance of the network is insignificant in comparison with droplets captured in the network. It was observed that droplets smaller than the pore throats have substantially lower capture rate than the ones of the size comparable to pore throats. The observed trend holds for the lower injection rate and concentrations as well. Droplets of 15 μm size did not show retention at any of the tested conditions for the monodisperse emulsion experiments.

Fig. 5a shows typical plugging configurations by 30 μm droplets that were observed at the tested conditions. The images show that the flow through a pore was restricted by a single droplet, or several droplets by the bridging mechanism as suggested in the literature from indirect observation (Moradi et al., 2014). Moreover, the observations suggest that bridging played a crucial role in the process of pore clogging by 30 μm droplets. The irregularities at the throat to pore body connection and the flow bifurcation created an upstream stagnation point at the entrance to a pore throat where a droplet was trapped and held by the wedging mechanism (Herzig et al., 1970). A subsequent droplet passing through the pore, bridged it by being trapped between the already retained droplet and the pore wall due to reduced effective area of the pore. The droplet capture configurations indicate that although 30 μm droplets underwent some degree of retention, the impairment caused by the droplets is negligible considering that there are 10,050 pores in the network. The majority of the pores remain completely open allowing unrestricted flow of injection fluid through the network (Fig. 5b).

The lack of retention events for 15 μm droplets indicates that the surfactant molecules could have created a strong repulsive energy barrier, which prevented droplet capture. This suggests that the interception mechanism had little to no role in the process of droplet capture for the tested systems. On the other hand, it is important to highlight that the surface of the used network is very smooth. This could have played a role in the absence of retention events for 15 μm droplets, as it was shown in the literature that surface roughness can also influence colloid retention by altering streamlines (Auset and Keller, 2006). Many reports in the literature used surfactant stabilized emulsion for the study of droplet transport through porous media and considered interception mechanism as one of the contributors to droplet capture (Błaszczyk et al., 2016; Moradi et al., 2014; Romero et al., 2011; Yu et al., 2018). The stabilization of emulsions gives a better control over experiments and prevents coalescence of droplets, which allows comparison of droplet size distribution at the inlet and outlet of a sample. However, the findings in this paper point out that the influence of surfactant on droplet-pore surface interaction might be significant and should be taken into account when planning this type of experiments.

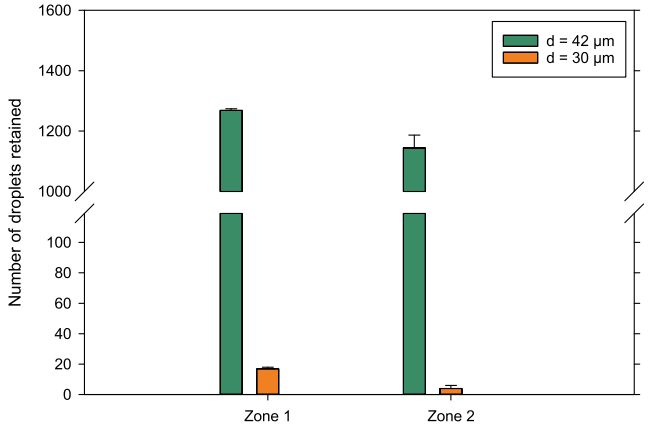


**Fig. 4.** Number of retained droplets in zone 1 and zone 2 for droplets of 30 μm and 42 μm size at 1500 ppm dispersed phase concentration and 4 μl/min flow rate.

On the other hand, flooding the micromodel with 42 μm droplets demonstrated severe impairment (Fig. 5c and Fig. 5d). The droplets were captured at the entrance into pore throats by straining mechanisms as suggested in the literature (Soo and Radke, 1986; Yu et al., 2018). The retained droplets experienced flow re-entry by two mechanisms: 1) *squeezing* through a pore throat due to the pressure difference across a pore; and 2) by being pushed through a pore due to the momentum gained from *collision* with a subsequent droplet. However, every single droplet that entered the network was eventually retained. Fig. 6 depicts the evolution of droplet retention over pore volumes injected. One can see that initially the droplets are retained only in zone 1. After 16 PV of flooding the number of retained droplets in zone 1 reached a plateau and started to fluctuate around the same value until the end of the experiment. Once zone 1 reached the plateau, droplet retention began in zone 2. After 34 PVs injected the number of retained droplets in zone 2 started to converge with the plateau of zone 1. This observation suggests that there was a droplet retention equilibrium, which once reached moves the retention front deeper into the network. This reasoning is substantiated by the simulation and experimental data reported in the literature (Buret et al., 2010; Jin and Wojtanowicz, 2017).

### 3.2. Flow rate

The results show that injection rate played a significant role on droplet retention both for 30 μm droplets and 42 μm droplets. For 30 μm the effect was on the retention rate, while for 42 μm the flow rate affected the retention equilibrium.

Fig. 7a shows that for 30 μm droplets at the concentration of 1500 ppm the retention is significantly lower at higher injection rates. This is associated with larger velocities at the stagnation point upstream the pillars, which reduced the probability of droplets being captured there. Another explanation is that subsequent droplets entering the pore had a larger velocity at the moment of collision with the already retained droplet; thus, the droplet gained enough momentum to re-enter the flow, which prevented the forming of bridges. Interestingly, for all injection rates, the number of retained droplets decreased from zone 1 to zone 2.

Fig. 8a compares the effect of flow rate on retention of large droplets at the oil concentration of 1500 ppm. The number of retained droplets in zone 1 at 4 μl/min is lower than at 2 μl/min. The difference arises from the flow re-entry mechanisms discussed in Section 3.1. The squeezing mechanism was dominant at 4 μl/min since the pressure drop across a clogged pore was higher than at 2 μl/min. The collision mechanism was more dominant at 2 μl/min; therefore, droplets percolated as they collided and pushed each other deeper into the network. The consequence of this differ-

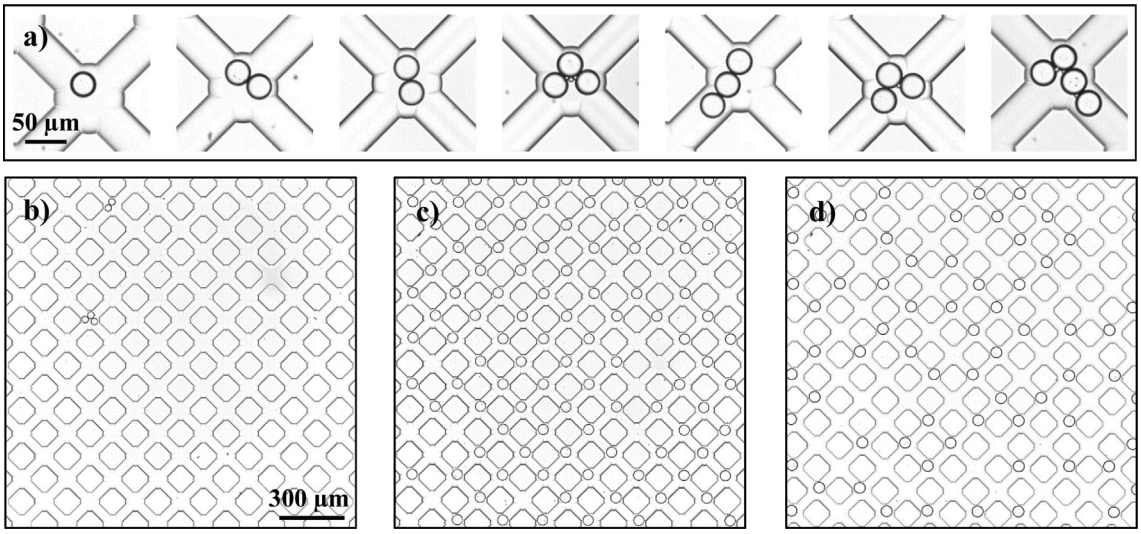


**Fig. 5.** Droplet retention instances for monodisperse emulsions: (a) typical configurations of 30 µm size droplets plugging the pores; (b) multi-pore scale view of the network during the flow of 30 µm droplets; (c) multi-pore scale view of the network during the transport of 42 µm droplets at the flow rate of 2 µl/min; and (d) multi-pore scale view of the network during the transport of 42 µm droplets at the flow rate of 4 µl/min.

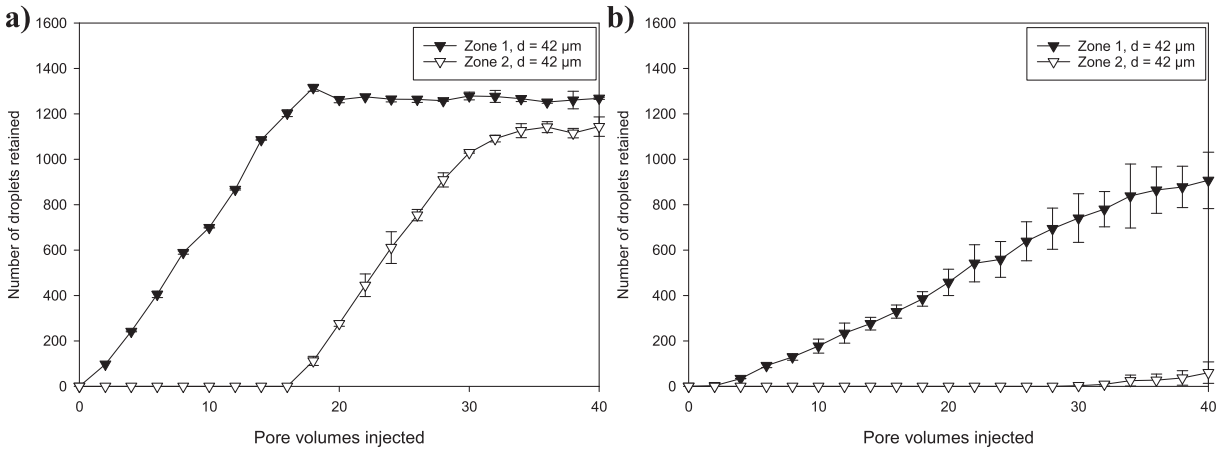


**Fig. 6.** The number of retained 42 µm droplets over 40 PVs of flooding at the flow rate of 4 µl/min and the dispersed phase concentration of: (a) 1500 ppm and (b) 500 ppm.

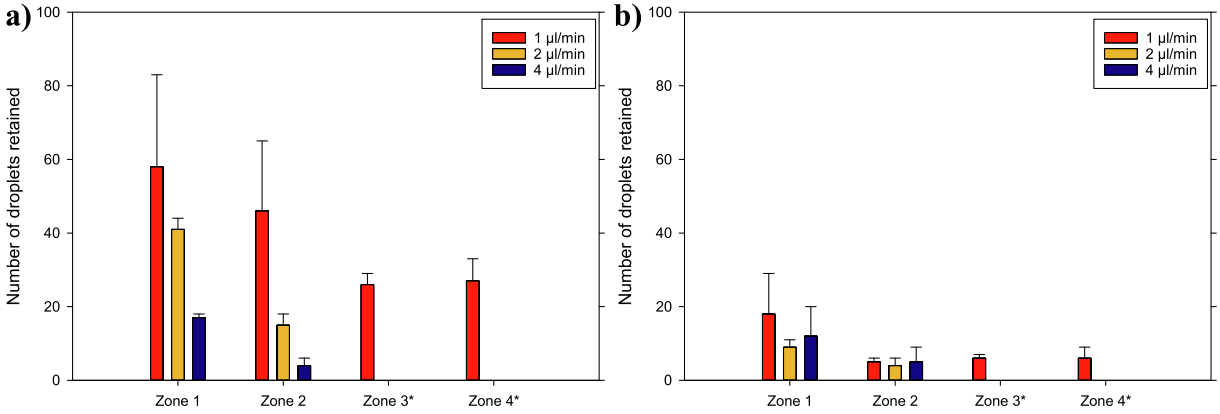


**Fig. 7.** The number of 30 µm droplets captured in the network after 40 PV of injection at the flow rates of 1 µl/min, 2 µl/min, 4 µl/min and the dispersed phase concentration of: (a) 1500 ppm and (b) 500 ppm. * Zone 3 and Zone 4 were not imaged at 2 µl/min and 4 µl/min flow rates.

ence can be visually inspected in Fig. 5c and Fig. 5d. At the lower injection rate, the local saturation of the network with droplets was larger than at the higher rate, which contributes to greater retardation of the flow and the blockage of streamlines. At 4 µl/min, the droplets percolated through the network quicker than at 2 µl/min filling about 50% of the pores in each zone; however,

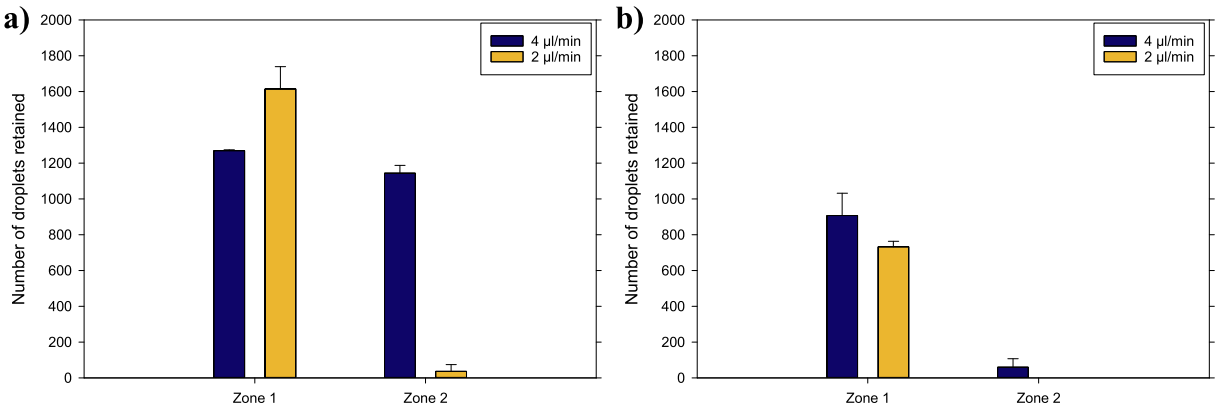


**Fig. 8.** The number of 42 µm droplets captured in the network after 40 PV of injection at the flow rates of 2 µl/min and 4 µl/min and the dispersed phase concentration of: (a) 1500 ppm; (b) 500 ppm.

the connectivity of pores was higher due to a less dense arrangement of the droplets, which maintained streamlines across the network. The flow velocities are important to consider in the context of the radial flow around a well bore since they decrease as the distance from the well increases (Jin and Wojtanowicz, 2017). This suggests that as the distance from the well bore increases the flow re-entry mechanisms would change. Closer to the well bore the squeezing mechanism would play the main role, while farther from the well the collision mechanism would dominate, and the packing of droplets become denser creating a ring of high oil saturation. Therefore, we hypothesize that an increase in the injection rate in order to push droplets through the pores would distance the ring from the wellbore delaying the injectivity decline; however, the decline is inevitable.

### 3.3. Dispersed phase concentration

The dispersed phase concentration played noticeable role in the size of obtained statistical sample and the possibility to draw conclusions from the results. Although the tested concentrations (500 ppm and 1500 ppm) are significantly higher than what is typically encountered during produced water re-injection (Mainguy et al., 2020; Martins et al., 1995; Rossini et al., 2020; Tipura et al., 2013), it was important to keep the concentrations high from the experimental point of view. Since the experiments were performed only up to 40 PVs to mitigate potential droplet coalescence or phase separation, emulsions with a low dispersed phase concentration would not provide large enough effect to reveal the trends as there were not enough droplets transported to the network. This can be distinctly seen in Fig. 8, where the results for 500 ppm and 1500 ppm of dispersed phase concentrations are compared. While the result depicted in Fig. 8a reflects the difference in the flow re-entry mechanisms at two different rates (by showing that there were more droplets retained in zone 1 than in zone 2 after 40 PVs), Fig. 8b does not allow to make this observation. Otherwise, if lower concentrations were used, experiments would have been performed for significantly more PVs, which could lead to changes in the emulsion properties during flooding. It is important to note that for both 500 ppm and 1500 ppm tests in total there are less droplets retained in the network at 2 µl/min flow rate than at 4 µl/min. This result is a consequence of a slightly larger velocity loss in the inlet channels at 2 µl/min flow rate in comparison with 4 µl/min (Figure S5); however, this drawback of the system still allows to perform a reasonable comparison. When it comes to the overall effect of the concentration on the number of retentions, for 42 µm droplets, it can be seen from the comparison of Fig. 6a and Fig. 6b that at lower concentration droplet deposition rate is lower, which is expected. Thus, the deposition equilibrium was reached later in the PVs injected. This observation points out that as long as the drop-to-pore size ratio is larger than one the network would be filled by droplets regardless of the dispersed phase concentration. This in turn highlights the importance of considering droplet size- and pore size distributions in conjunction when setting re-injection water specifications, which has been discussed in the literature (Evans, 1994; Rossini et al., 2020), but still not always taken into account during PWRI (Azizov et al., 2021).

An interesting observation was made in the experiments where 30 µm droplets were tested (Fig. 7a and b). It can be seen that at 500 ppm there are more droplets retained in zone 1 than zone 2, which is similar to 1500 ppm tests. However, unlike higher concentration experiments, there were no distinguishable trends observed within a specific zone at 500 ppm concentration. It can be seen from Fig. 7b that in zone 2 there is approximately the same number of droplets retained at each tested flow rate. There were more droplets retained in zone 1 at 1 µl/min rate than at 2 µl/min and 4 µl/min rate; however, 2 µl/min injection rate showed least retention events. This again can be associated with a very low number of retention events due to fewer droplets being injected.

### 3.4. Polydispersity

In this section the flow of polydisperse emulsion comprising droplets of three size classes, 15 µm, 30 µm and 42 µm, was investigated to examine the effect of polydispersity on the transport of droplets. The dispersed phase concentration was kept at 1500 ppm for all experiments while flow rates were 2 µl/min and 4 µl/min. The number of droplets in each size class was approximately the same. Fig. 9a and b visualize the retention of droplets at the external filter cake and deeper in the network respectively.

The number of retained droplets for each size class over 40 PVs of flooding are compared in Fig. 10. It can be seen from the figure that the droplets of all size classes experienced retention, which is in contrast to the experiments with monodisperse emulsions where droplets of 15 µm size showed no retention. There was significantly more of 15 µm droplets retained in zone 1 at 2 µl/min rate than at 4 µl/min. This can be explained by the fact that the external filter cake was more pronounced at the former rate, which caused the capture of a large number of 15 µm droplets at the cake as illustrated in Fig. 9a. At the latter flow rate, the filter cake was limited allowing more droplets to pass into the network. Moreover, 42 µm droplets demonstrated similar behavior as observed in monodisperse experiments. The squeezing mechanism dominated at 4 µl/min, while at 2 µl/min droplets percolated due to collisions,

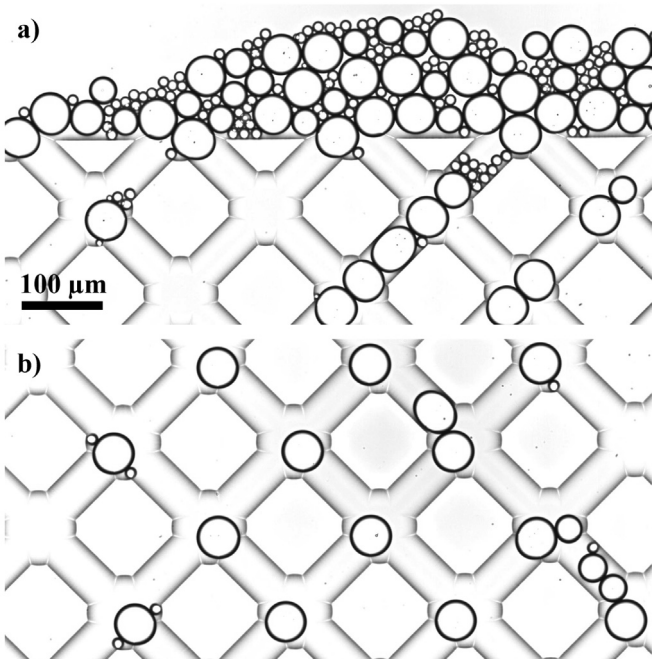


**Fig. 9.** Droplet retention instances for polydisperse emulsion at: (a) the filter cake; (b) deep in the network.

which resulted in a larger number of droplets retained in zone 1 at 2 µl/min rate than at 4 µl/min. However, similar to the experiments with monodisperse emulsions, very few droplets were trapped in zone 2 at the flow rate of 2 µl/min (Fig. 10b), while there were more droplets trapped in zone 1 at 2 µl/min than at 4 µl/min due to a denser packing. When it comes to 30 µm droplets, there were significantly more droplets retained in comparison with the monodisperse emulsion tests, although the number of droplets injected per PV was smaller in the polydisperse emulsion system. Fig. 10a shows that 15 µm and 30 µm droplets started to become trapped in zone 2 only after 42 µm droplets infiltrated into the zone. Moreover, as discussed in Section 3.2, the streamlines are not significantly blocked by 42 µm droplets at 4 µl/min rate, which would allow smaller droplets to pass to zone 2 from the beginning of the experiments. Therefore, it was hypothesized that 42 µm droplets was the facilitating factor for the capture of smaller droplets.

To scrutinize this idea every single retained droplet was examined for having a neighboring droplet within the same pore. Fig. 11a shows the share of retained droplets of each class that did not have a neighbor droplet, also referred to as independent retention. The figure illustrates that half of the captured 42 µm droplets at all examined flow rates belong to independent retention, while there were no such instances for the droplets of 15 µm, and only a small percentage of 30 µm droplets could be classified as such. Additionally, the droplets of 15 µm and 30 µm size were inspected for the size of their neighbors. Fig. 11b displays the percentage of 15 µm that had a neighbor droplet of 42 µm and/or 30 µm (droplets that had neighbors from only one or two size classes), and 42 µm & 30 µm at the same time (only droplets that had neighbors from two size classes). A similar graph for 30 µm can be found in the Supplementary Information (Fig. S6), with a comparable trend. It is seen from Fig. 11b that the majority of 15 µm droplets had an adjacent droplet of 42 µm, while the share of droplets that had 30 µm or 42 µm & 30 µm at the same time is comparable. This indicates that only a small share of 15 µm droplets had a single neighbor droplet that was of 30 µm size. These observations suggest that the retention of droplets smaller than the pore size was governed by their capture in the pores clogged by 42 µm droplets.

### 3.5. Evaluation of the approach

The presented method demonstrated feasibility of microfluidic approach for the investigation of emulsion transport in porous media, specifically considering dilute oil-in-water emulsions. In this paper, we established a systematic study of droplet retention at various conditions by controlling all the variables, including droplet sizes. Additionally, a pipeline for detecting captured droplets in flow was presented.

The method demonstrated several advantages and improvements compared to the reports in the literature. Firstly, the small fluid volumes needed to perform the microfluidic experiments allowed on-chip generation of emulsions, which in turn enabled usage of monodisperse and tailored polydisperse emulsions. Moreover, the usage of the glass funnel as the emulsion dispenser and on-chip generation of droplets enabled straightforward dilution of tailored emulsions to very low concentrations at a reasonable degree of repeatability. Previously, oil-in-water emulsions with a wide size distribution and high dispersed phase concentration were used to investigate emulsion propagation through micromodels (Liu et al., 2019b). When it comes to visualization, the method provided meticulous optical imaging and analysis of droplet retention at the pore-scale. Transparent cells, packed with beads or sand, provide reasonable macroscale visualization (Guillen et al., 2012a); however, pore-level visualization lacked systematic approach and allowed only qualitative analysis. More-

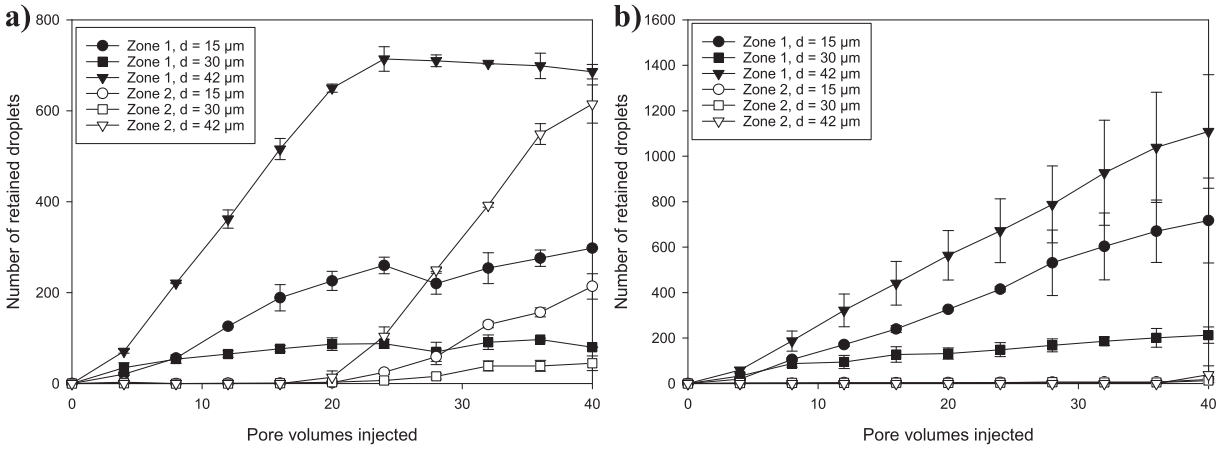


**Fig. 10.** The number of retained droplets for each size class (15 µm, 30 µm and 42 µm) over 40 PVs of injection at the flow rate of (a) 4 µl/min; and (b) 2 µl/min.

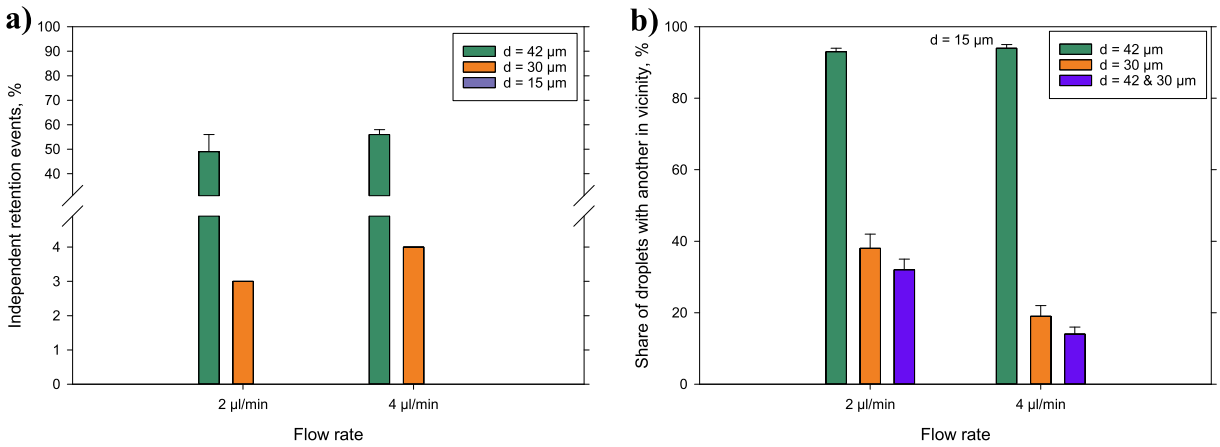


**Fig. 11.** Summary of polydisperse emulsion injection experiments. (a) percentage of retained droplets of each class having no neighbor within the same pore, or in other words independent retention events, at 2 µl/min and 4 µl/min rate; b) the share of 15 µm droplets that have a neighbour of 42 µm and/or 30 µm, and 42 µm & 30 µm size at the same time.

over, in comparison with micro-computed tomography, the method presents a "plug and play" experimental procedure at a relatively low cost.

On the other hand, there are some drawbacks that leave space for improvement of the method. First of all, the micromodels lacked minerology and surface roughness of pore walls, which are characteristic of a reservoir rock. The absence of the former eliminated pore wall-droplet interactions that would normally be present during core or sand pack flooding, while the latter could have influenced retention of 15 µm droplets as discussed in Section 3.1. Additionally, pore geometry was not representative of a rock, although this was done deliberately in order to obtain a benchmark for future studies (same holds for mineralogy). However, as discussed in Section 1, micromodels give a lot of possibilities in terms of altering their properties, which creates a great potential for future work with more realistic micromodels. When it comes to the issues associated specifically with the micromodel used here, the depth of the channels posed a great challenge and limited the conditions that could be tested, due to the squeezing of droplets. Another challenge that was identified during the development of the method is the potential influence of the inlet channels of the micromodel on the experiments. Although these channels provide uniform flow of fluids to the network, they could pose a problem if droplets are captured in these channels. This is a prospective problem for hydrophobic or functionalized micromodels when the surface of the channels is more favorable for droplet capture than in hydrophilic glass micromodels. Therefore, this should be taken into account when designing future experiments.

## 4. Conclusions

A microfluidic method to investigate the retention of droplets during the transport of dilute oil-in-water emulsions through porous media was presented. The use of micromodels allowed both qualitative and quantitative image-based analysis of retention events at pore-scale, which provided insights into the mechanisms and spatial distribution of the captured droplets. The experiments were performed using monodisperse emulsions of three droplet sizes (larger-, slightly smaller-, and significantly smaller than pore throats) and a polydisperse emulsion comprising the mentioned sizes. Moreover, various flow rates and two dispersed phase concentrations were tested. The experiments with monodisperse emulsions demonstrated that droplet size played a major role in the droplet retention process. It was observed that droplets slightly smaller than the pore throats showed very limited retention, while droplets that are significantly smaller demonstrated no capture at all. On the other hand, larger droplets experienced almost complete retention in the network. Furthermore, the flow rate tests revealed that the larger droplets percolated through pores by two mechanisms: collision and squeezing. The latter dominated at larger flow rate in the tested range, while the former at lower flow rate. The spatial analysis revealed that there is a retention equilibrium for the larger droplets, which causes the advancement of the retention front when it is reached. Additionally, data for the smaller droplets showed that at lower flow rates the droplets are more likely to be retained. Importantly, the dispersed phase concentration influenced the interpretation of the results. At lower concentration, the obtained statistical sample was not sufficiently significant to uncover any trends or differences between the tested conditions due to the limited number of pore volumes injected. The experiments with polydisperse emulsions demonstrated that droplets of all sizes were retained, as droplets larger than the pore throats facilitated retention of smaller droplets. The paper aimed to provide a microfluidic methodology for a systematic study of retention phenomenon. We believe that the presented method provides a solid ground for the future studies and provides flexibility for testing various emulsion systems in porous media for a range of applications, although some challenges were also identified.

## CRediT authorship contribution statement

**Ilgar Azizov:** Conceptualization, Methodology, Investigation, Data curation, Visualization, Writing – original draft. **Marcin Dudek:** Conceptualization, Methodology, Writing – review & editing, Project administration, Supervision. **Gisle Øye:** Conceptualization, Writing – review & editing, Project administration, Supervision.

## Declaration of Competing Interest

The authors declare that they have no known competing financial interests or personal relationships that could have appeared to influence the work reported in this paper.

## Acknowledgments

This work was carried out as a part of SUBPRO, a Research-based Innovation Centre within Subsea Production and Processing. The authors gratefully acknowledge the financial support from SUBPRO, which is financed by the Research Council of Norway, major industry

partners and NTNU. Additionally, the authors thank Jens Norrman and Sébastien Simon from NTNU for fruitful discussions.

## Appendix A. Supplementary material

Supplementary data to this article can be found online at https://doi.org/10.1016/j.ces.2021.117152.

## References


Abrams, A., 1977. Mud design to minimize rock impairment due to particle invasion. JPT. J. Pet. Technol. 29, 586–592. https://doi.org/10.2118/5713-PA.

Ali, M.A.J., Abeer, A.-F.A., Ali, A.-H.A., Suhaib, A.-K.A., 2011. The Effect of Suspended Solid Concentration and Oil Droplet Size Distribution on Particle Coalesces and Emulsion Stability. SPE/DGS Saudi Arab. Sect. Tech. Symp. Exhib. https://doi.org/10.2118/149028-MS

Atherton, T.J., Kerbyson, D.J., 1999. Size invariant circle detection. Image Vis. Comput. 17, 795–803. https://doi.org/10.1016/s0262-8856(98)00160-7

Auset, M., Keller, A.A., 2006. Pore-scale visualization of colloid straining and filtration in saturated porous media using micromodels. Water Resour. Res. 42. https://doi.org/10.1029/2005WR004639

Azizov, I., Dudek, M., Øye, G., 2021. Emulsions in porous media from the perspective of produced water re-injection – A review. J. Pet. Sci. Eng. 109057. https://doi.org/10.1016/j.petrol.2021.109057

Błaszczyk, M.M., Pacholski, P., Przybysz, Ł., Sęk, J., 2016. Influence of Granular Bed Parameters on Emulsion Flow and Elution Process of Oil-in-Water Emulsion. Tech. Sci. 19, 325–337.

Buret, S., Nabzar, L., Jada, A., 2010. Water Quality and Well Injectivity: Do Residual Oil-in-Water Emulsions Matter? SPE J. 15, 557–568. https://doi.org/10.2118/122060-PA.

Civan, F., 2007. Reservoir Formation Damage, Reservoir Formation Damage. Elsevier Inc. https://doi.org/10.1016/B978-0-7506-7738-7.X5000-3

Costier, L., van den Hoek, P.J., Davidson, C.J., Ding, M., van den Berg, J.T.M., Hofland, R., 2009. Establishing Water Injection Dynamics by Leading-Edge Coreflood Testing, in: EUROPEC/EAGE Conference and Exhibition. Society of Petroleum Engineers, pp. 8–11. https://doi.org/10.2118/121786-MS

Ding, B., Dong, M., Yu, L., 2020. A model of emulsion plugging ability in sandpacks: Yield pressure drop and consistency parameter. Chem. Eng. Sci. 211, 115248. https://doi.org/10.1016/j.ces.2019.115248.

Dudek, M., Chicault, J., Øye, G., 2020a. Microfluidic Investigation of Crude Oil Droplet Coalescence: Effect of Oil/Water Composition and Droplet Aging. Energy and Fuels 34 (5), 5110–5120. https://doi.org/10.1021/acs.energyfuels.9b0343410.1021/acs.energyfuels.9b03434.s001.

Dudek, M., Vik, E.A., Aanesen, S.V., Øye, G., 2020b. Colloid chemistry and experimental techniques for understanding fundamental behaviour of produced water in oil and gas production. Adv. Colloid Interface Sci. 276, 102105. https://doi.org/10.1016/j.cis.2020.102105.

European Commission, 2019. Best available techniques guidance document on upstream hydrocarbon exploration and production. Luxemborg.

Evans, R.C., 1994. Developments in Environmental Protection Related to Produced Water Treatments and Disposal (Produced Water Re-Injection). SPE Heal. Saf. Environ. Oil Gas Explor. Prod. Conf. https://doi.org/10.2523/27179-MS

Fakhru'l-Razi, A., Pendashteh, A., Abdullah, L.C., Biak, D.R.A., Madaeni, S.S., Abidin, Z. Z., 2009. Review of technologies for oil and gas produced water treatment. J. Hazard. Mater. 170, 530–551. https://doi.org/10.1016/j.jhazmat.2009.05.044

Guillen, V.R., Carvalho, M.S., Alvarado, V., 2012a. Pore Scale and Macroscopic Displacement Mechanisms in Emulsion Flooding. Transp. Porous Media 94 (1), 197–206. https://doi.org/10.1007/s11242-012-9997-9.

Guillen, V.R., Romero, M.I., Carvalho, M. da S., Alvarado, V., 2012b. Capillary-driven mobility control in macro emulsion flow in porous media. Int. J. Multiph. Flow 43, 62–65. https://doi.org/10.1016/j.ijmultiphaseflow.2012.03.001

Herzig, J.P., Leclerc, D.M., Goff, P.L., 1970. Flow of Suspensions through Porous Media—Application to Deep Filtration. Ind. Eng. Chem. 62, 8–35. https://doi.org/10.1021/ie50725a003

Jahanbakhsh, A., Wlodarczyk, K.L., Hand, D.P., Maier, R.R.J., Maroto-Valer, M.M., 2020. Review of Microfluidic Devices and Imaging Techniques for Fluid Flow Study in Porous Geomaterials. Sensors 20, 4030. https://doi.org/10.3390/s20144030.

Jin, L., Wojtanowicz, A.K., 2017. SPE-184411-MS An Analytical Model Predicts Pressure Increase During Waste Water Injection to Prevent Fracturing and Seismic Events.

Jin, Lu, Wojtanowicz, Andrew K, 2014. Progression of injectivity damage with oily waste water in linear flow. Pet. Sci. 11 (4), 550–562. https://doi.org/10.1007/s12182-013-0371-0.

van de Laar, T., ten Klooster, S., Schroën, K., Sprakel, J., 2016. Transition-state theory predicts clogging at the microscale. Sci. Rep. 6, 28450. https://doi.org/10.1038/srep28450.

Liu, Q., Zhao, B., Santamarina, J.C., 2019. Particle Migration and Clogging in Porous Media: A Convergent Flow Microfluidics Study. J. Geophys. Res. Solid Earth 124, 9495–9504. https://doi.org/10.1029/2019JB017813

Liu, Z., Li, Y., Luan, H., Gao, W., Guo, Y., Chen, Y., 2019b. Pore scale and macroscopic visual displacement of oil-in-water emulsions for enhanced oil recovery. Chem. Eng. Sci. 197, 404–414. https://doi.org/10.1016/j.ces.2019.01.001.

Mainguy, M., Perrier, S., Bure, E., 2019. Produced-Water Reinjection in Deep Offshore Miocene Reservoirs, Block 17, Angola. SPE Prod. Oper. Preprint, 1–16. https://doi.org/10.2118/197061-PA

Martins, J.P., Murray, L.R., Clifford, P.J., McLelland, W.G., Hanna, M.F., Sharp, J.W., 1995. Produced-Water Reinjection and Fracturing in Prudhoe Bay. SPE Reserv. Eng. 10, 176–182. https://doi.org/10.2118/28936-PA

Mendez, Z.D.C., 1999. Flow of Dilute Oil-in-Water Emulsions in Porous Media. University of Texas at Austion.

Mikolajczyk, G., Huang, L., Wilhelm, M., Dreher, W., Odenbach, S., 2018. Colloid deposition in monolithic porous media – Experimental investigations using X-ray computed microtomography and magnetic resonance velocimetry. Chem. Eng. Sci. 175, 257–266. https://doi.org/10.1016/j.ces.2017.09.054.

Moradi, M., Kazempour, M., French, J.T., Alvarado, V., 2014. Dynamic flow response of crude oil-in-water emulsion during flow through porous media. Fuel 135, 38–45. https://doi.org/10.1016/j.fuel.2014.06.025.

Ochi, J., Oughanem, R., 2018. An Experimental Investigation of Formation Damage Induced by PWRI in Unconsolidated Sands. SPE Int. Conf. Exhib. Form. Damage Control. https://doi.org/10.2118/189513-MS

Palsson, B., Davies, D.R., Todd, A.C., Somerville, J.M., 2003. The Water Injection Process. Chem. Eng. Res. Des. 81 (3), 333–341. https://doi.org/10.1205/02638760360596883.

Pang, S., Sharma, M.M., 1997. A Model for Predicting Injectivity Decline in Water-Injection Wells. SPE Form. Eval. 12, 194–201. https://doi.org/10.2118/28489-pa

Pradhan, S., Shaik, I., Lagraauw, R., Bikkina, P., 2019. A semi-experimental procedure for the estimation of permeability of microfluidic pore network. MethodsX 6, 704–713. https://doi.org/10.1016/j.mex.2019.03.025.

Romero, M.I., Carvalho, M.S., Alvarado, V., 2011. Experiments and network model of flow of oil-water emulsion in porous media. Phys. Rev. E 84, 46305. https://doi.org/10.1103/PhysRevE.84.046305.

Rossini, S., Roppoli, G., Mariotti, P., Renna, S., Manotti, M., Viareggio, A., Biassoni, L., 2020. Produced water quality impact on injection performance: Predicting injectivity decline for waterflood design. In: in: International Petroleum Technology Conference 2020, IPTC 2020. International Petroleum Technology Conference (IPTC). https://doi.org/10.2523/iptc-20013-ms.

Rousseau, D., Latifa, H., Nabzar, L., 2007. PWRI-Induced Injectivity Decline: New Insights On In-Depth Particle Deposition Mechanisms. Eur. Form. Damage Conf. https://doi.org/10.2118/107666-MS

Saadat, M., Tsai, P.A., Ho, T.H., Oye, G., Dudek, M., 2020. Development of a Microfluidic Method to Study Enhanced Oil Recovery by Low Salinity Water Flooding. ACS Omega. https://doi.org/10.1021/acsomega.0c02005

Saadat, Marzieh, Yang, Junyi, Dudek, Marcin, Øye, Gisle, Tsai, Peichun Amy, 2021. Microfluidic investigation of enhanced oil recovery: The effect of aqueous floods and network wettability. J. Pet. Sci. Eng. 203, 108647. https://doi.org/10.1016/j.petrol.2021.108647.

Sandengen, K., Kristoffersen, A., Melhuus, K., Jøsang, L.O., 2016. Osmosis as mechanism for low-salinity enhanced oil recovery, in. SPE Journal. Society of Petroleum Engineers, 1227–1235. https://doi.org/10.2118/179741-pa.

Schneider, M.H., Tabeling, P., 2011. Lab-on-chip methodology in the energy industry: Wettability patterns and their impact on fluid displacement in oil reservoir models. Am. J. Appl. Sci. 8, 927–932. https://doi.org/10.3844/ajassp.2011.927.932.

Soo, H., Radke, C.J., 1986. A filtration model for the flow of dilute, stable emulsions in porous media-I. Theory. Chem. Eng. Sci. 41 (2), 263–272. https://doi.org/10.1016/0009-2509(86)87007-5.

Souza, A.L.S., Figueiredo, M.W., Kuchpil, C., Bezerra, M.C., Siqueira, A.G., Furtado, C. A., 2005. Water Management In Petrobras: Developments And Challenges, in: Offshore Technology Conference. Offshore Technology Conference. https://doi.org/10.4043/17258-MS

Tipura, L., Tjomsland, T., Fagerbakke, A.-K., 2013. Increasing Oil Recovery on the Grane Field With Challenging PWRI. OTC Bras. https://doi.org/10.4043/24532-MS.

van Oort, E., van Velzen, J.F.G., Leerlooijer, K., 1993. Impairment by suspended solids invasion. Testing and prediction. SPE Prod. Facil. 8, 178–183. https://doi.org/10.2118/23822-pa.

Vaz, A., Bedrikovetsky, P., Fernandes, P.D., Badalyan, A., Carageorgos, T., 2017. Determining model parameters for non-linear deep-bed filtration using laboratory pressure measurements. J. Pet. Sci. Eng. 151, 421–433. https://doi.org/10.1016/j.petrol.2017.01.001.

Wyss, H.M., Blair, D.L., Morris, J.F., Stone, H.A., Weitz, D.A., 2006. Mechanism for clogging of microchannels. Phys. Rev. E 74,. https://doi.org/10.1103/PhysRevE.74.061402 061402.

Xu, Wei, Ok, Jeong Tae, Xiao, Feng, Neeves, Keith B., Yin, Xiaolong, 2014. Effect of pore geometry and interfacial tension on water-oil displacement efficiency in oil-wet microfluidic porous media analogs. Phys. Fluids 26 (9), 093102. https://doi.org/10.1063/1.489407110.1063/1.4894071.1.

Yu, Long, Ding, Boxin, Dong, Mingzhe, Jiang, Qi, 2018. Plugging Ability of Oil-in-Water Emulsions in Porous Media: Experimental and Modeling Study. Ind. Eng. Chem. Res. 57 (43), 14795–14808. https://doi.org/10.1021/acs.iecr.8b03805.

Yu, Long, Sang, Qian, Dong, Mingzhe, Yuan, Yanguang, 2017. Effects of Interfacial Tension and Droplet Size on the Plugging Performance of Oil-in-Water Emulsions in Porous Media. Ind. Eng. Chem. Res. 56 (32), 9237–9246. https://doi.org/10.1021/acs.iecr.7b01770.